VORTEX ENERGY CAPTURE USING A CANTILEVERED BEAM IN THE WAKE OF A BLUFF BODY

By

SARAH ELIZABETH SIGNAL

(Under the Direction of R. Benjamin Davis)

ABSTRACT

Fish are known to conserve energy by synchronizing their motion with vortices shed from a nearby object. In this thesis, the prospect of capturing energy from passing vortices to generate upstream propulsion is explored. The configuration of interest is a flexible cantilevered beam in the wake of a rigid cylinder. The system is simulated by modeling the vortices as loads that move down the length of beam at a given flow speed. The model is used to calculate the dynamic response of the beam. The results show that the beam's resonant response can be maximized when its length is equal to the diameter of the cylinder divided by the Strouhal number. Data from preliminary experiments conducted in a high-speed water tunnel are also presented. In separate experiments, a flexible beam and plate are placed in the wake of a cylinder and response data are collected using a laser Doppler vibrometer.

INDEX WORDS: Kármán vortex street, wake, fish, moving load model, cantilever beam, splitter plate, cylinder, propulsion

VORTEX ENERGY CAPTURE USING A CANTILEVERED BEAM IN THE WAKE OF A BLUFF BODY

By

SARAH ELIZABETH SIGNAL

B.S., The University of Georgia, 2016

A Thesis Submitted to the Graduate Faculty of The University of Georgia in Partial Fulfillment of the Requirements for the Degree

MASTER OF SCIENCE

ATHENS, GEORGIA

2018

VORTEX ENERGY CAPTURE USING A CANTILEVERED BEAM IN THE WAKE OF A BLUFF BODY

By

SARAH ELIZABETH SIGNAL

Major Professor: R. Benjamin Davis

Committee: Eric Freeman
C. Brock Woodson

Electronic Version Approved:

Suzanne Barbour
Dean of the Graduate School
The University of Georgia
December 2018

Acknowledgements

This thesis would not have been possible without the aid and support that I received from many people.

Foremost, I am grteful to each of the members of my Master's Advisory Committee along with the faculty and staff of the College of Engineering at the University of Georgia whom have provided me with educational guidance. I would especially like to thank Dr. R. Benjamin Davis for giving me this opportunity to extend my education. As my professor and mentor, he has taught me more than I could ever give him credit for here. I am profoundly grateful for his patience, motivation , enthusiasm, and immense knowledge. I would also like to extend a heartfelt thanks to my past and present labmates who gave me invaluable help with my research.

I gratefully acknowledge the funding received towards my master's degree from the Science, Mathematics, and Research for Transformation (SMART) Fellowship established by the Department of Defense. I am also grateful to the funding received through the College of Engineering's Research Assistantship program at the University of Georgia.

Nobody has been more important to me in the pursuit of this degree than the members of my family and close friends. Their continuous love and guidance are with me in whatever I pursue. To show my appreciation, this work is dedicated to my ultimate role models, my parents, Walter and Karen Signal.

Contents

Acknowledgements **iv**

List of Figures **vi**

Nomenclature **ix**

1 Introduction **1**

1.1 Fish in Periodic Flow 3

1.2 Contributions of the Thesis 7

2 Moving Load Model **8**

2.1 Background 9

2.2 Finite Element Beam Model 10

2.3 Results 15

3 Experimental Studies of Bodies Placed in the Wake of a Cylinder **22**

3.1 Performance of a Cantilever Beam in a Vortex Wake 22

3.2 Interaction Between a Splitter Plate and a Cylinder 27

4 Conclusions **35**

4.1 Summary of Main Results 35

4.2 Recommended Future Work 36

Bibliography **37**

List of Figures

2.1 A simplified schematic of a fish in the wake of a Kármán vortex street. The wake is represented by a moving load pattern of alternating forces, while the fish is idealized as a cantilever beam. 9

2.2 Strouhal Number of vortex shedding from a stationary smooth circular cylinder [1]. 16

2.3 The ratio of the displacement at the end of the cantilever beam behind a cylinder with a diameter of $D = 0.1$ m to the static displacement of a unit force at the end of a beam at **(a)** $StUr = 0.2$ **(b)** $StUr = 0.5$ **(c)** $StUr = 1.0$ **(d)** $StUr = 1.5$ **(e)** $StUr = 2.0$ **(f)** $StUr = 2.5$. The term $StUr$ is the reduced velocity multiplied by the Strouhal number with reduced velocity expressed as $Ur = \frac{U}{f_n D}$, where U is the flow speed and f_n is the natural frequency. The Strouhal number is held constant at 0.2. Here, the natural frequency for the beam's first mode is used. 17

2.4 The ratio of the displacement at the end of the cantilever beam behind a cylinder with a diameter of **(a)** $D = 0.08$ m **(b)** $D = 0.1$ m **(c)** $D = 0.2$ m to the static displacement of a unit force at the end of a beam. 18

2.5 The ratio of RMS values for displacement data at the end of a cantilever beam behind a cylinder with a diameter $D = 0.1$ m to the static displacement of a unit force at the end of the beam for ζ values of 0.01, 0.025, and 0.05 compared to the ratio of the length of the beam to load distance. Here, the distance between loads is held constant, while the length of the beam is varied. 19

2.6 Max deflection of a cantilever beam behind a cylinder normalized by the static displacement of a unit force at the end of the beam for various values of $\frac{L}{\Delta x}$. The length of the beam is held constant. The term Δx is expressed as $\Delta x = \frac{D}{St}$. The Strouhal number, St, is set at 0.2, while the diameter of the cylinder, D, is varied. 20

2.7 A square wave representative of a cantilever beam exposed to a moving load pattern of alternating forces traveling at a constant speed. 20

3.1 A cantilever beam with a chord length of 15.24 cm, span of 5.08 cm, and thickness 2.54 mm stationed behind a horizontally mounted cylinder with a diameter of 7.62 cm located in the test section of a water tunnel. 23

3.2 Response data from the end of a cantilever beam with a length of 25.4 cm, width of 7.62 cm, and thickness of 2.54 mm as fluid flow, U, is constantly accelerated over a range of 0.1458 m/s to 2.916 m/s. The response frequency is normalized by the beam's natural frequency. The term $StUr$ is the reduced velocity multiplied by the Strouhal number, St, with reduced velocity express as $Ur = \frac{U}{f_n D}$. The Strouhal number is assumed to be held constant at $St = 0.2$, and the diameter of the cylinder is $D = 7.62$ cm. . . . 25

3.3 RMS values of the experimental velocity data taken at the end of a cantilever beam with a length of 15.24 cm, width of 5.08 cm, and thickness of 2.54 mm for flow speeds varied from 0.43 m/s to 3.63 m/s in increments of $).21$ m/s. The Strouhal number is assumed to be held constant at a value of 0.2. 27

3.4 RMS values of the experimental velocity data sets taken at the end of a plate with a length and width of 14.25 cm and a thickness of 2.41 mm attached to a cylinder with a diameter of 2.85 cm and length of 14.25 cm. The flow speed is varied from 0.44 m/s to 3.8 m/s in increments of 0.15 m/s. 30

3.5 Dye visualization of a plate with a length and width of 14.25 cm and thickness of 2.41 mm attached to a cylinder with a diameter of 2.85 cm and length of 14.25 cm at a flow speed of 0.1 m/s 31
3.6 Drag coefficient values for the present cylinder compared to that of a smooth and rough cylinder from a previous study [2]. The present cylinder has a diameter of 2.85 cm and length of 14.25 cm. The drag force of the cylinder is measured over a flow speed range of 0.44 m/s to 3.8 m/s. 33
3.7 Drag coefficient values for a bare cylinder with a length of 14.25 cm and diameter of 2.85 cm and a plate with a length and width of 14.25 cm and thickness of 2.41 mm attached to a cylinder with a length of 14.25 cm and diameter of 2.85 cm over a flow speed range of 0.44 m/s to 3.8 m/s. 33

Nomenclature

Δt	Time between forces
Δt_e	Amount of time a force spends on an element
Δx	Distance between forcing loads
η	Generalized coordinates
λ	Natural frequency parameter
$[\Phi]$	Normal mode matrix
$[C]$	Damping matrix
$[K]$	Global stiffness matrix
$[K_e]$	Element stiffness matrix
$[M]$	Global mass matrix
$[M_e]$	Element mass matrix
$\{F\}$	Force vector
$\{x\}$	Displacement vector in physical coordinates
ν	Viscosity
ω	Natural frequencies
ρ_f	Density of fluid
ρ_s	Structural density
ζ	Modal damping
A	Beam deflection
A_0	Beam deflection due to a static unit load

b	Beam width
C_D	Drag coefficient
D	Diameter of the cylinder
E	Young's Modulus
F	Force amplitude
f	Forcing frequency
f_0	Fundamental frequency
$F_{D,CP}$	Drag force for the cylinder and plate
$F_{D,C}$	Drag force for the bare cylinder
$f_{n,v}$	Natural frequency in vacuum
f_n	Natural frequency
f_{vs}	Shedding frequency
h	Beam thickness
I	Moment of inertia
L	Beam length
L_e	Length of each element
L_C	Length of cylinder
M	Structural mass
m	Mass per unit length
M_a	Added mass
N	Number of modes
N_e	Number of elements
St	Strouhal number
T	Time between like sign loads encountering the beam
T_{vs}	Vortex shedding period
U	Flow speed
Ur	reduced velocity

Chapter 1

Introduction

Live fish are able to conserve energy by synchronizing their body to vortices shed by a nearby object. By capturing energy from the passing vortices, the fish can sometimes remain stationary or propel themselves forward without expending muscle energy [3–5]. There has been significant interest in developing devices designed to mechanically imitate fish behavior, with the goal of designing vehicles that are faster, more energy efficient, and less detectable than traditional underwater vehicles [6].

Different species of fish have different swimming styles. Webb [7] identified one of the main swimming styles as body and/or caudal fin (BCF) propulsion. This describes species that swim by creating wave-like movements with their body. BCF propulsion is divided into five subcategories: anguilliform, subcarangiform, carangiform, thunniform, and ostraciiform. Species belonging to each of these categories swim with a varying amount of body movement. Anguilliform locomotion consists of a full-body undulatory motion while carangiform locomotion typically uses one-third of the body for swimming, and thunniform locomotion uses only the caudal fin or tail for propulsion [8]. Prior work has mainly focused on studying the wake of fish with subcarangiform locamotion, such as trout [3,5,9], and carangiform locamotion, such as bluegill sunfish [10, 11]. These locomotion forms are most commonly studied using thrust or power as a metric for comparison [12–15].

Many studies have endeavored to simplify hydrodynamic environments in an attempt to better understand the complex motions associated with swimming. Early studies assessed the swimming motion of fish in still water or uniform flow [16, 17]. As models became more complex, conflicting evidence arose surrounding the effects of turbulence on swimming fish, primarily looking at whether fish are attracted to or repelled by turbulence. At extremely high levels of turbulence, the metabolic cost of swimming can be increased and shear stresses can even damage the bodies of fish, but it has also been shown that altered flows that maintain periodicity can be exploited by fish and reduce energy requirements associated with swimming. This energy reduction shows that energy costs, previously estimated using steady flow conditions, must account for the effects of complex flow. In general, non-periodic, turbulent flow that produces large fluctuations in velocity tends to repel fish, while periodic fluctuations can attract fish. Non-periodic turbulent flows tend to require powered movements from fish to maintain propulsion, while periodicity can lead to passive propulsion through altering posture of the body and fins. With advancing technologies, real-time measurements of energy expenditure can be obtained. Electromyography (EMG) transmitters have been inserted into fish and calibrated to tail-beat frequencies and swimming speeds, which can be correlated to oxygen consumption and muscle activity. An alternative method of analyzing the metabolic cost of fish swimming is to measure the pressure changes along the body of the fish to determine power production. However, natural velocity gradients in the flow may make it difficult to accurately interpret the data. Expanding simple hydrodynamic environments to include environmental effects and determining how these effects influence fish biomechanics is important to establishing a better understanding of how fish use environmental conditions to their benefit [18].

1.1 Fish in Periodic Flow

Fish encounter vortices in their environment from fluid flowing past stationary objects or the movements from other animals. It is believed that fish often exploit these vortices by extracting energy from them to increase their swimming performance. In fact, salmon and trout migrate to optimal positions within streams to maximize their net energy gain [19]. Beal [4] later conducted an experiment to further this idea by finding the optimal position and testing whether the amount of expended energy used to swim was reduced at this position. Because of the possibility to capture energy from cylinder vortices, rainbow trout are allowed to freely swim in the presence of a vertically mounted D-section cylinder. A D-section cylinder is used because in flow it is able to produce a Kármán wake, with stronger vortices than a circular cylinder and has a Strouhal number of approximately 0.2 [20]. In the experiment, the fish are allowed to find the cylinder's wake on their own. The trout adapted to the presence of the cylinder fairly quickly, and in each iteration of the experiment, the trout slowly moved upstream until they were approximately $4D$ downstream from the cylinder [4].

In a similar experimental setup, Liao et al. [3] found that trout synchronize their tail-beat frequency to the vortex shedding frequency of the cylinder and adopt a locomotion termed the Kármán gait. Here, the vortex shedding frequency is defined as $St = \frac{fD}{U}$. Liao et al. went even further in their experiment and studied the muscle activity of the trout swimming by using fine wire electrodes to record electrical muscle activity. They found that opposed to the pattern of propagating muscle activity the trout experiences from swimming in free stream, trout only activate their anterior, axial muscles when they adopt the Kármán gait. In other words, the trout display a significant reduction in muscle activity when they are entrained behind the cylinder rather than swimming in free stream, implying that the trout are using the vorticity for energy benefit.

To prove that the trout are stationing themselves in this position for energy benefits and not just taking advantage of the wake's velocity deficit, tests were conducted with euthanized fish that had to overcome their drag using only the oscillating flows in the wake as energy input. In an experiment, conducted by Beal et al. [5], a line was hooked to the fish and tied to a stationary D-sectioned cylinder. The fish was held taut $4D$ downstream of the cylinder. This decision was based on the range in which the live fish were seen to hold station in the previous experiment. Results showed that the dead fish synchronized with the wake and moved upstream until it ran into the cylinder. These experiments were able to prove conclusively that fish were extracting energy from the vortices and, essentially, were able to rest behind the cylinder. Additionally, the dead fish's frequency closely matched that of the wake. This is in agreement with results from Liao et al. [3].

More recently, Lauder et al. [21] conducted a study to examine the passive swimming capabilities of freshly dead fish bodies. It was ensured that rigor mortis had not set in during the experiments. The body was attached to a robotic flapping mechanical device and actuated in heave and pitch in various combinations. Similar body waveforms to that of live trout were able to be generated by the passive fish bodies. The data showed that heave had the greater effect on swimming performance than pitch. As the driving frequency of the mechanical device was increased from 0.1 to 4.5 Hz, the tail beat amplitude remained relatively constant from 0.1 to 2 Hz before increasing steadily to a peak at 3.5 Hz. This increase in tail beat amplitude of the magnitude shown in the results is comparable to those observed from live fish as they increase their swimming speed and alter both frequency and amplitude of their tail beat.

Gopalkrishnan et al. [20] investigated the effect that spacing between a cylinder and an oscillating foil has on the efficiency of the foil and the possibility of energy extraction. The foil is placed in the wake of a D-section cylinder, and the testing range begins about $3D$ downstream from the cylinder as not to interfere with the formation of vortices. The cylinder is towed at a constant speed generating a Kármán vortex street and forced to os-

cillate with a displacement of $y(t) = A_c sin\,(2\pi f_c t)$ where A_c is the oscillation amplitude of the cylinder and f_c is the oscillation frequency. The tests were performed with three different cylinder oscillation amplitude ratios, $A_c/D = 0.500, 0.667$, and 0.833 where D is the diameter of the cylinder. These values were chosen to ensure strong vortex shedding lock-in. From the results distinct peaks and hollows can be identified, which implies that foil efficiency is highly dependent on the separation length between the cylinder and foil. Here, efficiency is defined as $\eta_F = \frac{T_{hF}U}{P_F}$ where T_{hF} is the average thrust force acting on the foil, U is the free stream velocity, and P_F is the average power input to the foil. The first peak is at about $4.3D$, which coincides with Beal's [4] later finding that live fish station themselves about $4D$ downstream from a D-section cylinder. Additionally, the presence of the peaks and hollows suggests that the oscillating foil interacts with the vortices in the Kármán street. If there was no interaction, the efficiency of the foil would decrease as the spacing between the cylinder and foil increased. The peaks in the efficiency are associated with the foil extracting energy from the oncoming cylinder eddies. Further, the peaks represent a 'destructive interaction' meaning the cylinder vortices encounter vortices of the opposite sign shed by the foil, and the cylinder vortices are repositioned, and ultimately, weakened. Similarly, the hollows represent a 'constructive interaction' where the cylinder vortices merge with vortices of the same sign shed by the foil to form much stronger vortices.

Having earlier established a dead fish's capability to extract energy and generate thrust from its interaction with a Kármán wake, Beal tested whether a mechanical device was able to produce a similar effect. Following the same procedure as Gopalkrishnan et al. [20], but instead using an oscillating D-section cylinder, a passive foil is tested moving through an unsteady drag wake. A potentiometer is used to record the instantaneous lift, thrust, torque, and pitch positions for the foil. Based on the measured phase angle, length of separation between the cylinder and foil, and the motion of the foil, the foil adopts a slaloming mode by avoiding intercepting the oncoming cylinder eddies. The resulting wake consists of two

vortices, one from the cylinder and the other from the foil. The foil is able to extract energy from the flow and generate enough thrust to overcome its drag. Liao et al. [3] discovered this same slaloming mode in live fish. The slaloming mode is a high-efficiency mode employed by both live fish and mechanical foils [5].

With the possibility of mechanical devices generating thrust proven, more recent work has looked into how it is influenced by different traits. For example, using flexible plastic foils, experiments are conducted to analyze the effects of shape, length, and stiffness on self-propelled swimming speed. These foils are driven at their leading edge by a computer-controlled robotic flapper and swim in a recirculating flow tank. The plastic foils are made to exhibit key characteristics of undulatory locomotion in freely-swimming fish. Lauder et al. [22] found that length has a non-linear effect on the foil's self-propelled swimming speed. Changing the stiffness was also shown to have non-linear changes in speed as the length of the foil was increased. Essentially, there is no simple relationship between self-propelled swimming speed and length or stiffness of the foils. Furthermore, experimental results suggest that the flexible foils are experiencing a resonance phenomenon in which certain lengths interact with the moving fluid in a manner that enhances propulsion, while other lengths interact in a negative manner that decreases swimming speed. Due to limitations of the testing space, a two-dimensional inviscid analytical model of the swimming foils was created to calculate self-propelled swimming speeds for a wider range of lengths. Results show that to correctly interpret the swimming performance among different self-propelling bodies requires knowledge of both the stiffness and length of the body. Lauder et al. [22] also tested five different foil shapes to determine its effect on propulsion. They found that shape alone is not a primary determinant of swimming hydrodynamics. Instead active control of fin stiffness is an important component of thrust magnitude.

1.2 Contributions of the Thesis

While prior studies have focused on fish swimming in steady flow [7, 17], the analysis on the hydrodynamic response of fish to oncoming vortices is relatively new due to complexity involved. A simplified analytical model is created to provide physical insight and a preliminary experiment is conducted as a first step toward understanding how to design systems to efficiently capture vortex energy.

- **Chapter 2:** With analogies to an anguilliform swimmer in a periodic wake, this chapter models the case of a flexible cantilevered beam subject to a periodic moving load. The intent is to capture the salient features of the response of flexible structures in vortical flows without a lot of complexity and computational expense.

- **Chapter 3:** This chapter experimentally considers the hydrodynamic interaction between a cylinder and an attached, flexible, downstream splitter plate over a range of Reynolds number from 12,400 to 108,000. The experiment has some similarities to fish swimming in the wake of bluff bodies and also is considered as a benchmark test of a new force balance system.

Chapter 2

Moving Load Model

This chapter develops a moving load model to capture the salient aspects of the dynamic response of a cantilever beam subject to vortex induced excitation. Because previous work has shown that fish generate optimal thrust in the wake of a Kármán street [23, 24], the model seeks to simulate this wake pattern. A Kármán wake is the periodic detachment of pairs of alternate vortices shed off a bluff body. A bluff body is a general term used for a body that, because of its shape, separates flow over most of its surface; an example is a cylinder. For this model, the wake is represented by a moving load pattern of alternating forces, as seen in Fig. 2.1. This model is similar to the 'moving force' models, seen in previous works [25–27], which are often used to model the interaction between vehicles and bridges. Results from the model will be used to guide the design of forthcoming experiments.

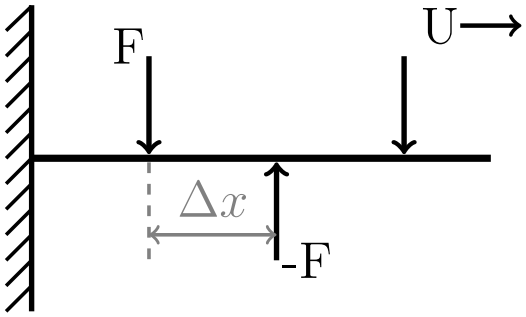

Figure 2.1. A simplified schematic of a fish in the wake of a Kármán vortex street. The wake is represented by a moving load pattern of alternating forces, while the fish is idealized as a cantilever beam.

2.1 Background

The response of structures excited by a moving force has been of great interest to many researchers involved in the analysis of railroad bridges and highway structures. In 1996, Esmailzadeh and Ghoreyshi [28] used a finite difference algorithm to study the dynamic behavior of a Timoshenko beam carrying a moving mass. The equations of motion are converted to equivalent finite difference equations of motion and solved. Increasing the length of the load distribution decreases the maximum deflection of the beam.

In a similar study, a Timoshenko beam is subject to a moving mass with a constant velocity. The beam is discretized into a number of simple elements, each with four degrees of freedom. The inertial effects of the moving mass are used to build a finite element model. Using direct integration on the equations of motion, the dynamic response of the Timoshenko beam and the contact force can be obtained. Lou et al. [29] found that the results from this study matched well with those in other literature.

In another study, Bilello et al. [30] investigated the dynamic response of a small-scale bridge model under a moving mass. The analysis is based on the continuous Euler-Bernoulli beam theory. By expanding the unknown structural response in a series of eigenfunctions, the given problem is reduced to a set of second-order linear differential equations with time varying coefficients. A scale model experiment is conducted to validate the ana-

lytical results. A prototype of a single span bridge structure with a smooth roadway is built and subjected to a vehicle traversing it at constant velocity. Results show that the analytical approach compared well with the experiment.

While many studies assumed that the moving mass and beam always remained in contact, Lee [31] believed that separation between the two occurs. His study assumed that the interaction force between the mass and structure depends on both the velocity of the moving mass and the flexibility of the structure. He analytically investigated a Bernoulli-Euler beam subject to a single mass at a constant velocity. By using the integro-differential equation and modal analysis, Lee found that separation between the beam and moving mass can occur easily and affects the dynamic response of the beam, especially at high velocities.

Because moving load models are usually used to study bridges, roadways, and railways, prior work has mostly involved fixed-fixed beams. This work is unique in that it considers the moving load problem on a cantilever beam.

2.2 Finite Element Beam Model

The problem is first solved by dividing the beam into a defined number of elements. Assume a cantilever beam of length L, width b, and thickness h is subject to a moving load. The equation of motion for an element of the beam is given by

$$[M]\{\ddot{x}\} + [C]\{\dot{x}\} + [K]\{x\} = \{F\}, \tag{2.1}$$

where $\{x(t)\}$ is a vector of displacements in physical coordinates, $[M]$ is the global mass matrix, $[C]$ is the damping matrix, $[K]$ is the global stiffness matrix, and $\{F\}$ is the force vector.

The structural element mass matrix is defined as [32]

$$[M_e] = \frac{mL_e}{420}\begin{bmatrix} 156 & 22L_e & 54 & -13L_e \\ 22L_e & 4L_e^2 & 13L_e & -3L_e^2 \\ 54 & 13L_e & 156 & -22L_e \\ -13L_e & -3L_e^2 & -22L_e & 4L_e^2 \end{bmatrix}, \tag{2.2}$$

where m is the mass per unit length

$$m = \rho_s bh, \tag{2.3}$$

and L_e is the length of each element

$$L_e = \frac{L}{N_e}, \tag{2.4}$$

with ρ_s being the structural density and N_e being the number of elements. The structural element stiffness matrix is defined as [32]

$$[K_e] = \frac{EI}{L_e^3}\begin{bmatrix} 12 & 6L_e & -12 & 6L_e \\ 6L_e & 4L_e^2 & -6L_e & 2L_e^2 \\ -12 & -6L_e & 12 & -6L_e \\ 6L_e & 2L_e^2 & -6L_e & 4L_e^2 \end{bmatrix}, \tag{2.5}$$

with E being Young's modulus and I the moment of inertia of the beam, $I = \frac{bh^3}{12}$. Both the structural element mass and stiffness matrices are two node elements modeling displacement and rotational degrees of freedom at each node. The global matrices $[M]$ and $[K]$ are computed using direct assembly. To illustrate the assembly process, assume the beam in Fig. 2.1 is divided into three elements; the global mass and stiffness matrices for the model are shown. Because the lengths of elements are the same, the global stiffness matrix can be constructed and simplified to

$$[M] = \frac{mL_e}{420}\begin{bmatrix} 156 & 22L_e & 54 & -13L_e & 0 & 0 & 0 & 0 \\ 22L_e & 4L_e^2 & 13L_e & 3L_e^2 & 0 & 0 & 0 & 0 \\ 54 & 13L_e & 312 & 0 & 54 & -13L_e & 0 & 0 \\ -13L_e & -3L_e^2 & 0 & 8L_e^2 & 13L_e & -3L_e^2 & 0 & 0 \\ 0 & 0 & 54 & 13L_e & 312 & 0 & 54 & -13L_e \\ 0 & 0 & -13L_e & -3L_e^2 & 0 & 8L_e^2 & 13L_e & -3L_e^2 \\ 0 & 0 & 0 & 0 & 54 & 13L_e & 156 & -22L_e \\ 0 & 0 & 0 & 0 & -13L_e & -3L_e^2 & -22L_e & 4L_e^2 \end{bmatrix}.$$

The global stiffness matrix $[K]$ is assembled in a similar manner. The global stiffness matrix for the model in Fig. 2.1 is expressed as

$$[K] = \frac{EI}{L_e^3}\begin{bmatrix} 12 & 6L_e & -12 & 6L_e & 0 & 0 & 0 & 0 \\ 6L_e & 4L_e^2 & -6L_e & 2L_e^2 & 0 & 0 & 0 & 0 \\ -12 & -6L_e & 24 & 0 & -12 & 6L_e & 0 & 0 \\ 6L_e & 2L_e^2 & 0 & 8L_e^2 & -6L_e & 2L_e^2 & 0 & 0 \\ 0 & 0 & -12 & -6L_e & 24 & 0 & -12 & 6L_e \\ 0 & 0 & 6L_e & 2L_e^2 & 0 & 8L_e^2 & -6L_e & 2L_e^2 \\ 0 & 0 & 0 & 0 & -12 & -6L_e & 12 & -6L_e^2 \\ 0 & 0 & 0 & 0 & 6L_e & 2L_e^2 & -6L_e & 4L_e^2 \end{bmatrix}.$$

The damping matrix, $[C]$, can be found by a modal analysis procedure in which damping is first neglected. The undamped equation of motion for the system is

$$[M]\{\ddot{x}\} + [K]\{x\} = \{F\}. \tag{2.6}$$

By substituting $\{x\} = [\Phi]\{\eta\}$ into Eq. (2.6) and premultiplying the equation by $[\Phi]^T$ the modal coordinates of Eq. (2.6) can be written

$$[\Phi]^T[M][\Phi]\{\ddot{\eta}\} + [\Phi]^T[K][\Phi]\{\eta\} = [\Phi]^T\{F\}, \tag{2.7}$$

where η is used to denote the modal degrees of freedom and $[\Phi]$ is the mass normalized mode matrix. Since $[\Phi]^T [M] [\Phi]$ is then identity matrix and $[\Phi]^T [K] [\Phi]$ is a diagonal matrix of natural frequencies squared, ω^2, Eq. (2.7) becomes

$$\{\ddot{\eta}\} + \begin{bmatrix} \omega_1^2 & & \\ & \ddots & \\ & & \omega_N^2 \end{bmatrix} \{\eta\} = [\Phi]^T \{F\}, \tag{2.8}$$

where N is the number of modes. With the equations uncoupled in modal space, damping can now be added back to the system in the form

$$\ddot{\eta}_i + 2\zeta_i \omega_i \dot{\eta}_i + \omega_i^2 \eta_i = \{\Phi_i\}^T \{F\} \qquad i = 1, 2, 3, ...N \tag{2.9}$$

where ζ_i is the modal damping. The damping matrix is composed of the term $2\zeta_i\omega_i$ along its diagonal. The Newmark-β method is then used to numerically integrate the problem in modal coordinates. The system response is then transformed back into physical coordinates using the mode matrix.

2.2.1 Construction of the Force Matrix

The construction of the force matrix depends on the distance between loads, Δx, which varies with the vortex shedding period, T_{vs}. The vortex shedding period can be found from the vortex shedding frequency

$$f_{vs} = \frac{StU}{D}, \tag{2.10}$$

where St is the Strouhal number, U is the flow speed, and D is the diameter of the cylinder. With period being the inverse of frequency, the vortex shedding period is

$$T_{vs} = \frac{D}{StU}. \tag{2.11}$$

Now, Δx can be expressed in terms of T_{vs}

$$\Delta x = T_{vs} U. \tag{2.12}$$

Substituting Eq. (2.11) into Eq. (2.12), Δx becomes

$$\Delta x = \frac{D}{St}. \tag{2.13}$$

Eq. (2.13) shows that Δx, the distance between two like-sign vortices, depends on the diameter of the cylinder and St. This finding is in agreement with Liao et al. [3]. They also found the wake wavelength, or vortex spacing, was strongly dependent on cylinder diameter.

At each time step, a spatial forcing vector is defined and the individual forcing vectors are assembled into a matrix $[F_M]$; the force matrix for one positive force in Fig. 2.1 can be seen below.

$$F_M = \overset{\text{time step}}{\longrightarrow} \begin{bmatrix} F & 0 & 0 \\ 0 & F & 0 \\ 0 & 0 & F \end{bmatrix} \Big\downarrow \text{space step}$$

The beam is exposed to alternating forces with a distance of Δx between them. The forces are then consecutively superimposed into one matrix, F_T, with a spacing of Δt.

$$F_T = \begin{bmatrix} F & \dots & 0 & \overbrace{0 & \dots & 0}^{\Delta t} & -F & \dots & 0 & \\ \vdots & \ddots & \vdots & \vdots & \ddots & \vdots & \vdots & \ddots & \vdots & \dots \\ 0 & \dots & F & 0 & \dots & 0 & 0 & \dots & -F & \end{bmatrix}$$

In the numerical integration, the integration time step is set to Δt_e, so the force matrix can be assembled using diagonal submatrices. Essentially, Δt defines the time between the forces and is expressed as

$$\Delta t = \frac{\Delta x}{U \Delta t_e}, \tag{2.14}$$

where Δt_e is the amount of time the force spends on each element which is given by

$$\Delta t_e = \frac{L}{N_e U}. \tag{2.15}$$

2.3 Results

2.3.1 Time Domain Response

In this analytical experiment, a beam of length 0.5 m, width 0.075 m, and thickness 0.0025 m is placed behind a cylinder with a diameter of 0.05 m. The density of the beam, ρ_s, is 900 kg/m^3. The Young's Modulus, E, of the beam is 1.7×10^9 N/m^2. The beam is divided into 100 elements and the first ten modes are used in the analysis. The modal damping ratio is assumed to be 0.01 across all modes.

The moving load represents a vortex street. For a smooth cylinder, a vortex street forms only for a range of $40 < Re < 3 \times 10^5$ [33]. Yet, the model can assume a moving load for any value of U. The Strouhal number changes with Reynolds number; however, the change in St associated within the range of Reynolds numbers of most interest,10^3 and 10^5, is minimal, so the change can be neglected, as seen in Fig. 2.2. For this study, St is held constant at 0.2.

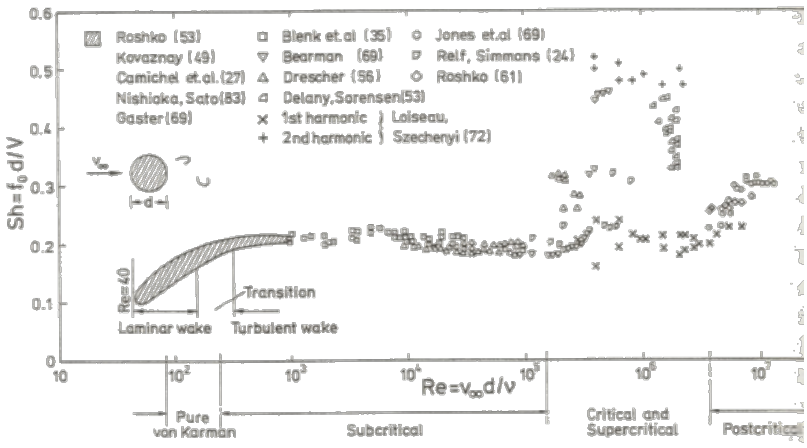

Figure 2.2. Strouhal Number of vortex shedding from a stationary smooth circular cylinder [1].

For low flow speeds, the force can be seen moving on and off the beam(see Fig. 2.3). As the force moves along the beam, the beam has time to decay in amplitude before it grows in amplitude in response to encountering another force. At higher flow speeds, the beam responds at a constant amplitude. Resonance is seen at $StUr = 2$. The term $StUr$ is the reduced velocity multiplied by St with reduced velocity expressed as

$$Ur = \frac{U}{f_n D}, \tag{2.16}$$

where f_n is the first natural frequency of the beam in hertz. In this study the natural frequency for the beam's first mode is used.

Because resonance is seen at $StUr = 2$, the results for the time histories at the end of the beam at $StUr = 2.0$ for $D = 0.08$ m, $D = 0.1$ m, and $D = 0.2$ m are analyzed (see Fig. 2.4). As the flow speed increases, T_{vs} decreases. When $D = 0.2$ m, the ratio of the length of the beam to load distance, $\frac{L}{\Delta x}$, is 0.5. At this ratio the beam is exposed to multiple forces at once. However, when $\frac{L}{\Delta x} = 1.25$, a force leaves the beam before the subsequent force comes into contact with the beam.

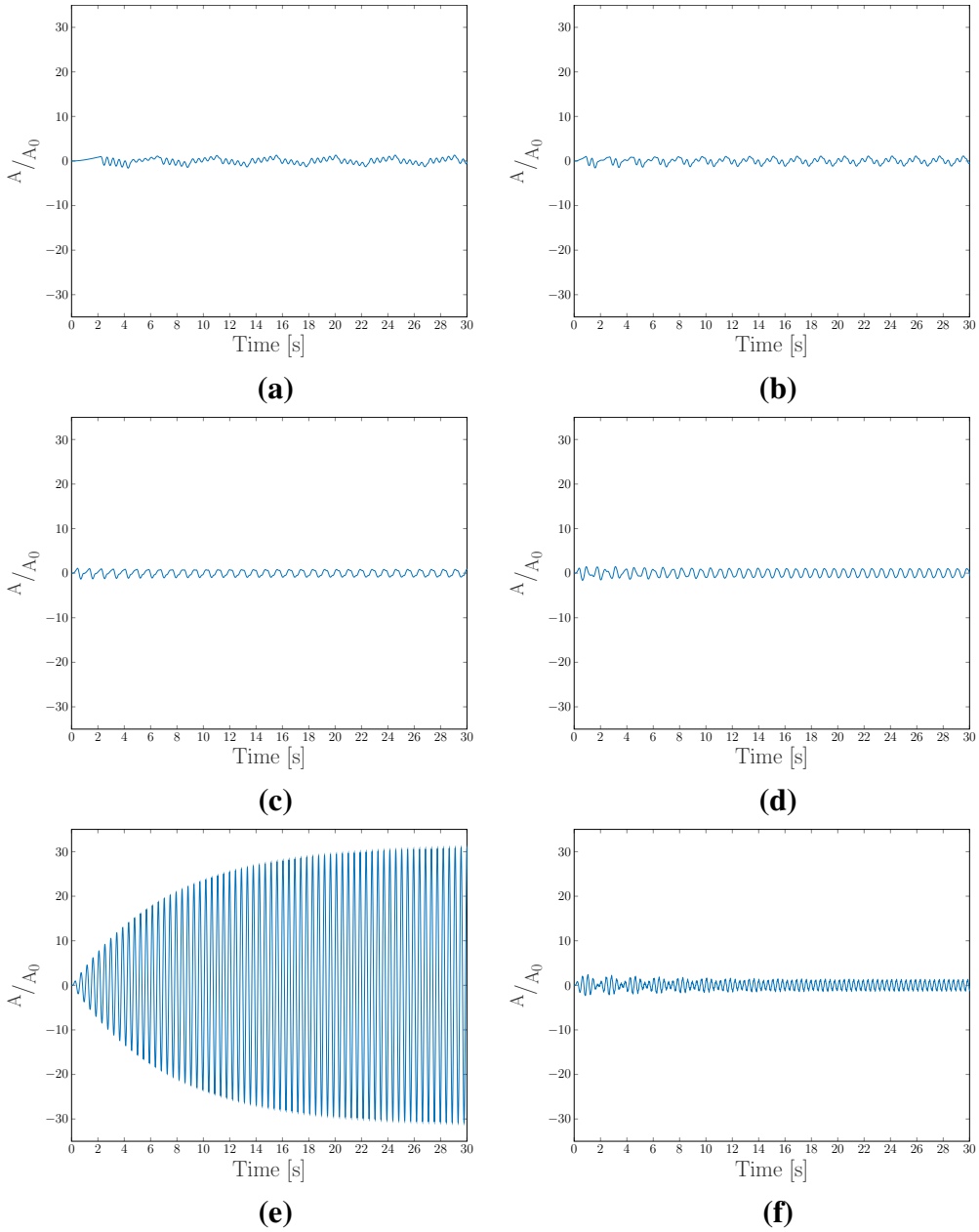

Figure 2.3. The ratio of the displacement at the end of the cantilever beam behind a cylinder with a diameter of $D = 0.1$ m to the static displacement of a unit force at the end of a beam at **(a)** $StUr = 0.2$ **(b)** $StUr = 0.5$ **(c)** $StUr = 1.0$ **(d)** $StUr = 1.5$ **(e)** $StUr = 2.0$ **(f)** $StUr = 2.5$. The term $StUr$ is the reduced velocity multiplied by the Strouhal number with reduced velocity expressed as $Ur = \frac{U}{f_n D}$, where U is the flow speed and f_n is the natural frequency. The Strouhal number is held constant at 0.2. Here, the natural frequency for the beam's first mode is used.

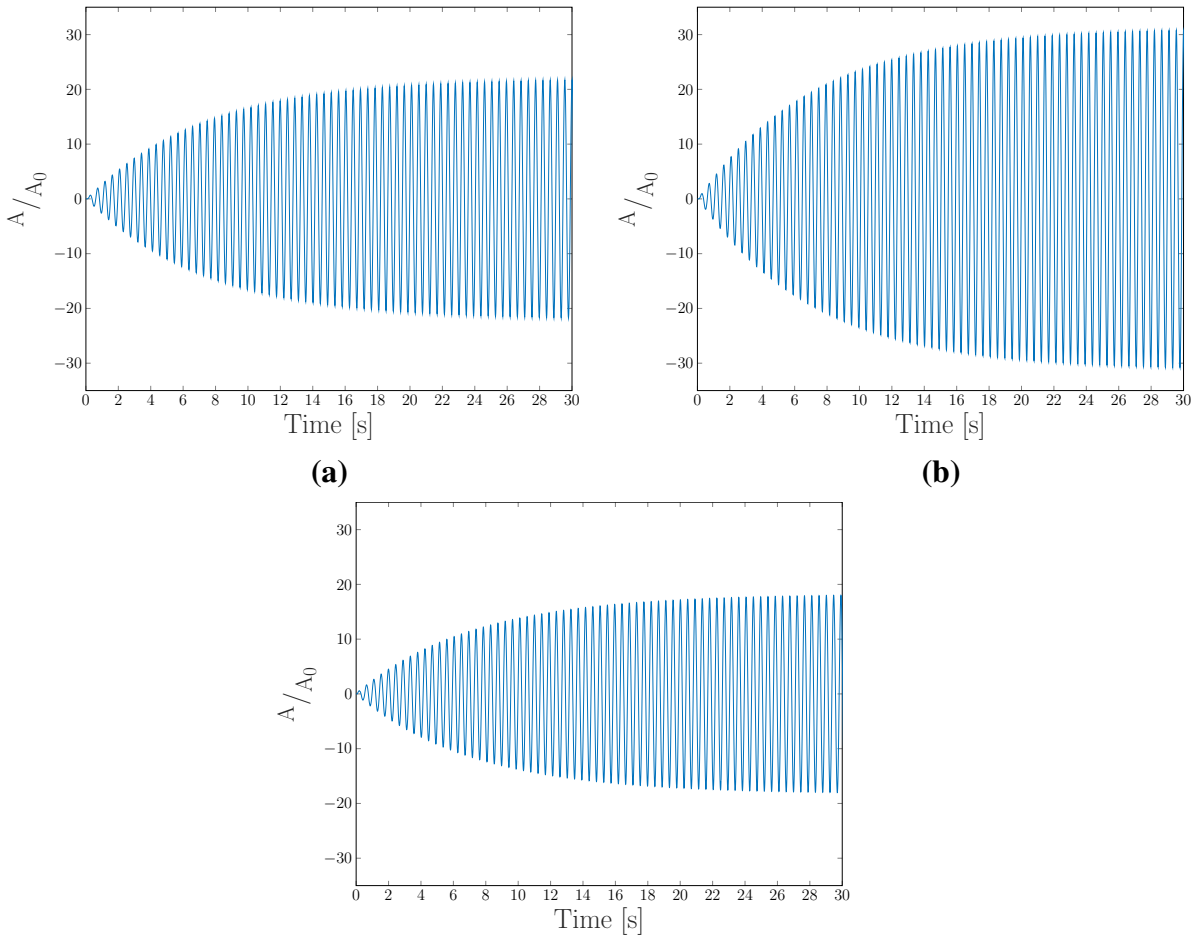

Figure 2.4. The ratio of the displacement at the end of the cantilever beam behind a cylinder with a diameter of **(a)** $D = 0.08$ m **(b)** $D = 0.1$ m **(c)** $D = 0.2$ m to the static displacement of a unit force at the end of a beam.

2.3.2 Frequency Domain Response

The RMS displacement values in Fig. 2.5 show a peak at $\frac{L}{\Delta x} = 1$ before decaying. This is in agreement with Fig. 2.6, as $\frac{\Delta x}{L} = 1$ produces the greatest peak amplitude.

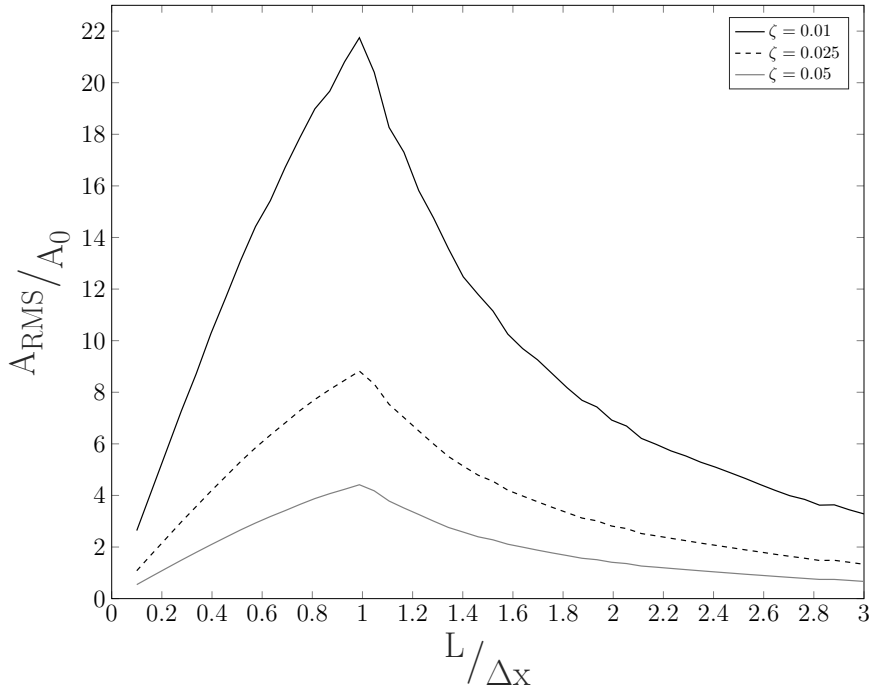

Figure 2.5. The ratio of RMS values for displacement data at the end of a cantilever beam behind a cylinder with a diameter $D = 0.1$ m to the static displacement of a unit force at the end of the beam for ζ values of 0.01, 0.025, and 0.05 compared to the ratio of the length of the beam to load distance. Here, the distance between loads is held constant, while the length of the beam is varied.

Fig. 2.6 shows the max displacement, A_{max}, for various $\frac{\Delta x}{L}$. A_{max} is normalized by the deflection due to a static unit load at the end of the beam, which is defined as

$$A_0 = \frac{FL^3}{3EI}, \tag{2.17}$$

where F is the force on the beam's tip. In Fig. 2.6, displacement peaks at $StUr = 2$ for all values of $\frac{L}{\Delta x}$. A second peak, lower in amplitude, is located at $StUr = 0.667$. This trend resembles the magnitude spectrum of the Fourier series of a square wave, because the moving load model's similarity to a square wave, as seen in Fig. 2.7.

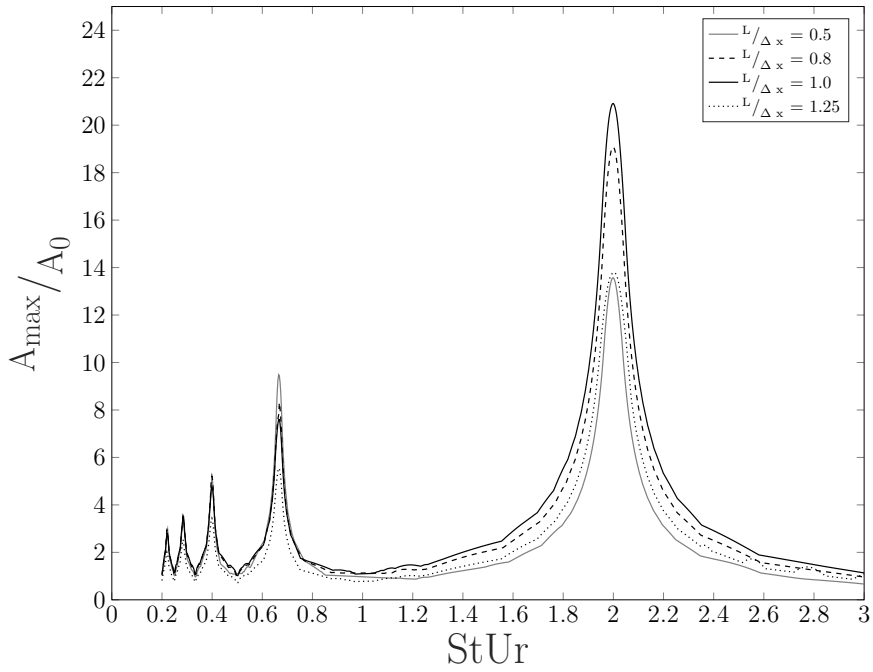

Figure 2.6. Max deflection of a cantilever beam behind a cylinder normalized by the static displacement of a unit force at the end of the beam for various values of $\frac{L}{\Delta x}$. The length of the beam is held constant. The term Δx is expressed as $\Delta x = \frac{D}{St}$. The Strouhal number, St, is set at 0.2, while the diameter of the cylinder, D, is varied.

A square wave alternates between two levels at regular intervals. For example, turning the signal on and off at regular intervals of period, T. The transitions between the two levels is instantaneous.

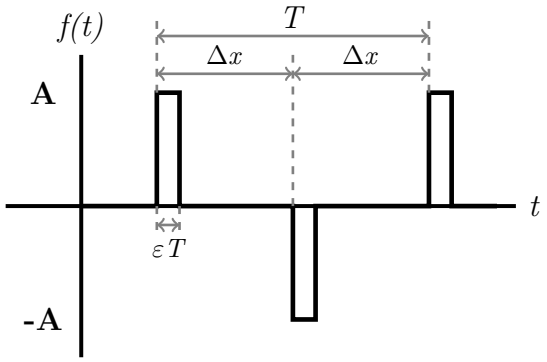

Figure 2.7. A square wave representative of a cantilever beam exposed to a moving load pattern of alternating forces traveling at a constant speed.

In the model, the load being introduced to and leaving the beam resembles a signal being turned on and off. An element encounters a force for a time, εT. The time between the first and secondary loads coming in contact with the beam is defined as Δx. The model is composed of forces with alternating signs. Consequently, the time between like sign loads encountering the beam is $2\Delta x$ or T. The fundamental frequency can be defined as

$$f_0 = 2f_{vs}. \tag{2.18}$$

Similar to a square wave, the present forcing function contains content at odd integer harmonics, (i.e, 3, 5, 7,...). Because the fundamental frequency is two times the vortex shedding frequency and $StUr$ is based on the vortex shedding frequency, the content produces sub-harmonic resonances at $StUr$ values of 0.66, 0.4, 0.286, $etc.$

Chapter 3

Experimental Studies of Bodies Placed in the Wake of a Cylinder

3.1 Performance of a Cantilever Beam in a Vortex Wake

Based on the configuration in Chapter 2 a set of experiments are designed to physically model Fig. 2.1. As with the analytical model, a flexible body is placed in the wake of a Kármán street for optimal thrust generation. To produce this wake pattern, a cylinder is horizontally mounted in fluid flow (see Fig. 3.1). Two test cases are considered; the first case studies a cantilever beam of chord length $L = 25.4$ cm, span $b = 7.62$ cm, and thickness $h = 2.54$ mm, while the second case observes a cantilever beam of chord length $L = 15.24$ cm, span $b = 5.08$ cm, and thickness $h = 2.54$ mm.

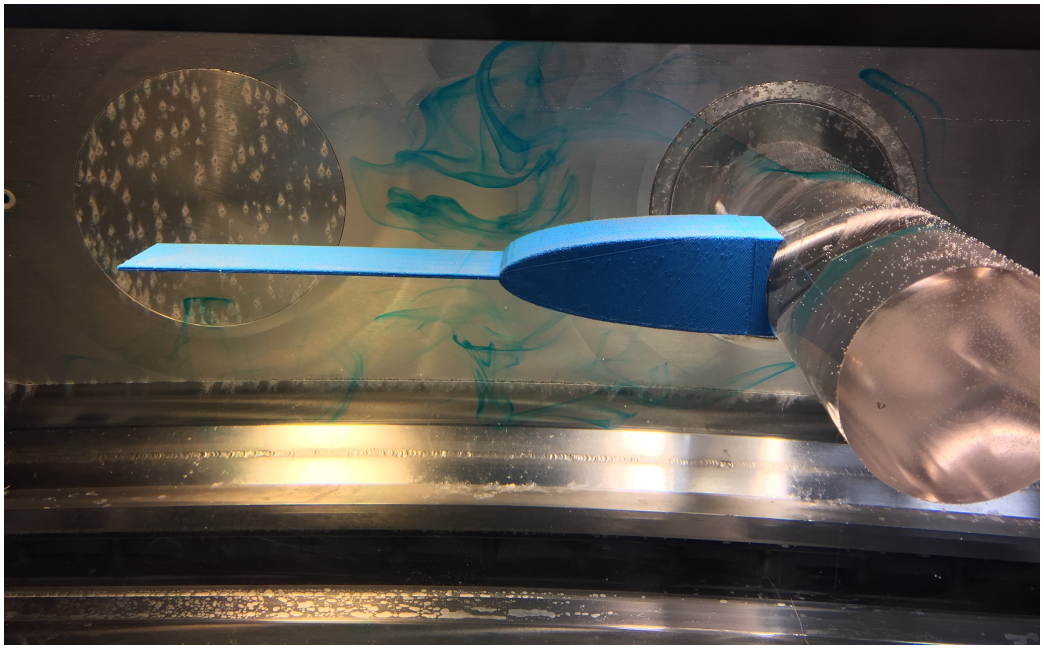

Figure 3.1. A cantilever beam with a chord length of 15.24 cm, span of 5.08 cm, and thickness 2.54 mm stationed behind a horizontally mounted cylinder with a diameter of 7.62 cm located in the test section of a water tunnel.

3.1.1 Experimental Set-Up

The cantilever beam ($E = 1.70 \times 10^9$ N/m^2, $\rho = 900$ kg/m^3) is used as a proxy for an eel. An attachment head, designed as not to disrupt fluid flow, is used to place the flexible beam behind a cylinder with diameter, $D = 7.62$ cm. The beam and attachment head are 3D printed as a single piece with a Makerbot Replicator 5th Gen using PLA filament. The fluid natural frequency of the structure, f_n, is found using the equation for natural frequency of a cantilever beam in fluid [1]

$$f = \frac{\lambda^2}{2\pi L^2}\sqrt{\frac{Eh^3}{12\rho_s h + 3\pi\rho_f b}} \tag{3.1}$$

where λ^2 is a natural frequency parameter dependent on the mode, boundary conditions, and dimensions of the beam. For the first mode of a fixed-free beam, $\lambda = 1.875$. The fluid natural frequency for the first case is $f_n = 1.65$ Hz; the cantilever beam in the second case has a fluid natural frequency $f_n = 5.6$ Hz. The structure's fluid natural frequency can be

controlled by its input parameters, h, b, and L. Values for these parameters are selected to ensure the beam will resonate with the vortex shedding frequency, shown in Eq. (2.10), while the von Kármán vortex street is still present. Since the von Kármán vortex street is desired the Reynolds number must be limited to a range of $40 < Re < 3 \times 10^5$ [33]. The flow speed relating to the desired Reynolds number range is found to be 0 m/s $< U <$ 2.63 m/s for a cylinder with a diameter of 7.62 cm.

3.1.1.1 High-Speed Water Tunnel

All tests are conducted in a high-speed water tunnel located in the Dynamic Devices and Solutions Lab at the University of Georgia. The tunnel is able to produce uniform flow as high as 11 m/s. The tunnel's test section is 1 m long with a 0.3×0.3 m^2 cross-section. The tunnel contains a honeycomb, upstream of the test section, that serves as a flow straightener to minimize the effects of turbulence of the incoming flow; as a result, the turbulence intensity of the flow outside of the boundary layer is about 0.5% [34].

3.1.1.2 Laser Doppler Vibrometer

A laser Doppler vibrometer (LDV) is a primary tool for data collection. A LDV focuses a laser beam on a test article, and the structure scatters or reflects the light from the laser. The back-scatter is demodulated using interference and the Doppler effect to measure vibration velocity at a point. The LDV is chosen because of its non-contact nature and ability to produce high resolution measurements. A LDV also has a larger measurement range than other available non-contact lasers.

3.1.2 Case 1

A cantiliever beam of chord length $L = 25.4$ cm, span $b = 7.62$ cm, and thickness $h =$ 2.54 mm is stationed behind a a cylinder with a diameter of 7.62 cm. Using an LDV, the

displacement at the end of the beam is observed as the fluid flow is constantly accelerated over a range of 0.1458 m/s to 2.916 m/s.

3.1.2.1 Results

Figure 3.2 shows the response data results in a scatter plot modeled after a spectrogram. The response frequency is normalized by the natural frequency of the beam. The Strouhal number is assumed to remain constant at a value of $St = 0.2$. The colors represent the deflection of the beam with lighter colors depicting higher amplitude. At low speeds, the body tries to vibrate at its natural frequency. However, once the flow speed increases the body is forced to vibrate at the forcing frequency. At higher speeds the body begins to vibrate at random frequencies. At these higher speeds, the wake is no longer in a Kármán street pattern, so the vortices display a sporadic pattern.

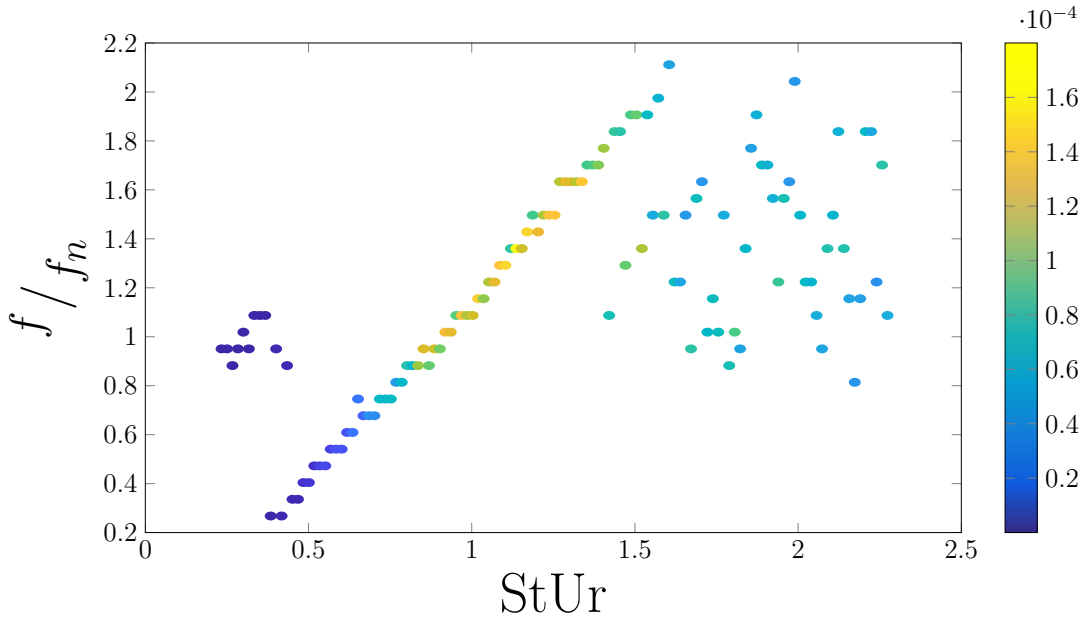

Figure 3.2. Response data from the end of a cantilever beam with a length of 25.4 cm, width of 7.62 cm, and thickness of 2.54 mm as fluid flow, U, is constantly accelerated over a range of 0.1458 m/s to 2.916 m/s. The response frequency is normalized by the beam's natural frequency. The term $StUr$ is the reduced velocity multiplied by the Strouhal number, St, with reduced velocity express as $Ur = \frac{U}{f_n D}$. The Strouhal number is assumed to be held constant at $St = 0.2$, and the diameter of the cylinder is $D = 7.62$ cm.

3.1.3 Case 2

The beam in Section 3.1.2 is replaced with a cantiliever beam of chord length $L = 15.24$ cm, span $b = 5.08$ cm, and thickness $h = 2.54$ mm. The beam is exposed to a constant flow speed, and using an LDV, the response data is measured at the end beam. The flow speed is varied from 0.43 m/s to 3.63 m/s in increments of 0.21 m/s. New response data is collected at each flow speed.

3.1.3.1 Results

The RMS value of each data set is found and plotted in Fig. 3.3. The Strouhal number in the term $StUr$ is assumed to be held constant at $St = 0.2$. Distinctive peaks and hollows can be seen in Fig. 3.3. As with Fig. 2.6, the data in Fig. 3.3 increases, reaches a peak, and then decreases before increasing again. This pattern is repeated throughout the data. The trend in Fig. 3.3 is similar to that found in Fig. 2.6 wherein the function contains content at odd integer harmonics. The max peak can be seen at $StUr = 1.5$ with a secondary peak located at $StUr = 0.53$. The location of these peaks differs from that found in Fig. 2.6. It is thought that the assumed value of the Strouhal number in the experimental study is incorrect.

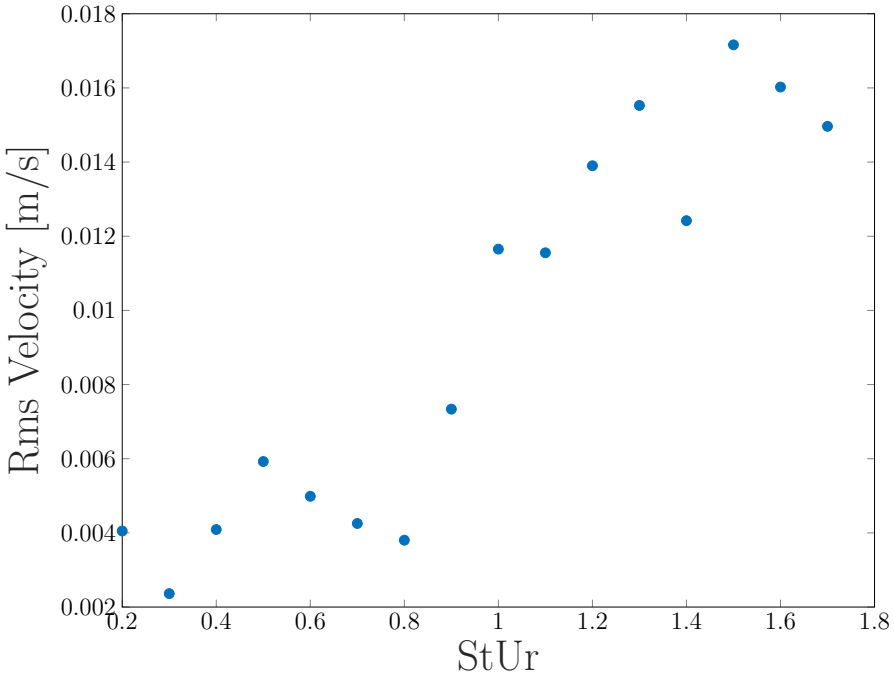

Figure 3.3. RMS values of the experimental velocity data taken at the end of a cantilever beam with a length of 15.24 cm, width of 5.08 cm, and thickness of 2.54 mm for flow speeds varied from 0.43 m/s to 3.63 m/s in increments of $).21$ m/s. The Strouhal number is assumed to be held constant at a value of 0.2.

3.2 Interaction Between a Splitter Plate and a Cylinder

This chapter experimentally studies a splitter plate attached to a cylinder. This configuration can be loosely compared to a fish swimming in the immediate wake of a cylinder. In earlier work Wu and Shu [35] numerically modeled a swimming tadpole using a rigid flat plate attached to a cylinder to study the effect the flapping tail had on the wake of the cylinder. They found that when the length of the plate equaled the diameter of the cylinder, the drag forces on the system is dependent on the plate amplitude and frequency; when the length of the plate is less than the diameter, a periodic variation of drag coefficients appeared at moderate and high plate frequency. This current study extends this topic by investigating a case where the length of the plate is larger than the diameter. Additionally,

Wu and Shu only considered a Reynolds number of 100. Here, the effects of a splitter plate on a cylinder are observed over a Reynolds number range of $12{,}000$ to $108{,}000$.

Testing is done with a force balance and dye injection system. These tools were recently constructed and installed. The experiments in this chapter were designed not only to investigate the hydrodynamic relationship between a splitter plate and cylinder but also to test the new force balance and dye injection systems that will be used in future vortex energy capture experiments.

3.2.1 Experimental Set-up

A flexible plate ($E = 1.7 \times 10^9$ N/m^2, $\rho_s = 900$ kg/m^3) with size $a = 14.25$ cm and thickness $h = 2.41$ mm is attached to a cylinder with diameter $D = 2.85$ cm and $L_C = 14.25$ cm. The geometry of the model was chosen to ensure accurate measurements at low speeds, see Section 3.2.3.1. The cylinder and beam are 3D printed as a uniform piece with a Makerbot Replicator 5th Gen using PLA filament. A bare cylinder of same length and diameter is also printed for comparison testing.

The structure's fluid natural frequency, f_n, of the model can be found by using the equation for the natural frequency of a cantilevered plate in fluid [36]

$$\frac{f_n}{f_{n,v}} = \frac{M^{1/2}}{(M_a + M)^{1/2}} = \frac{1}{\sqrt{1 + M_a/M}}, \tag{3.2}$$

where $f_{n,v}$ is the natural frequency in vacuum, M is the structural mass, and M_a is the added mass. The natural frequency in vacuum is defined as [36]

$$f_{n,v} = \frac{\lambda^2}{2\pi a^2} \left[\frac{Eh^2}{12\rho_s (1 - \nu)} \right]^{1/2}, \tag{3.3}$$

where ν is viscosity. For the first mode of a fixed-free plate with a length-width ratio of 1, $\lambda^2 = 3.492$. The add mass of a cantilevered plate is given by [36]

$$M_a = \frac{1}{4}\pi\rho_f a b^2 \tag{3.4}$$

where ρ_f is the density of the fluid and b is the width of the plate. For the current plate $a = b$. The fluid-loaded natural frequency of the test plate is predicted to be 3.61 Hz.

3.2.2 Structural Dynamic Measurements

3.2.2.1 Method

The cylinder and the plate are secured horizontally in the test section and subjected to a constant flow speed. Response data is taken at the tip of the plate with an LDV. The flow speed is varied from 0.44 to 3.8 m/s in increments of 0.15 m/s. At each flow speed, a new set of response data from the plate is collected.

3.2.2.2 Results

From the figure, the plate does not appear to be interacting with the shedding vortices of the cylinder (Fig. 3.4). Instead, the velocity of the plate increases with speed, seemingly, responding to turbulent excitation, the intensity of which increases with flow speed. While the amplitude of velocity generally increases with Reynolds number, there are drops in magnitude for some values of Reynolds numbers, and for the Reynolds number range of $70{,}000$ to $83{,}000$ the velocity is nearly constant. Shukla et al. [37] observed a similar trend in their work with a flexible splitter plate in the wake of a cylinder. They found that the splitter plate experiences two regimes of periodic motion known as mode I and mode II separated by a regime of non-periodic motion. Mode I is associated with a linear increase in plate deflection, while at mode II the plate maintains a constant amplitude. The current data seems to be constantly alternating between the two modes.

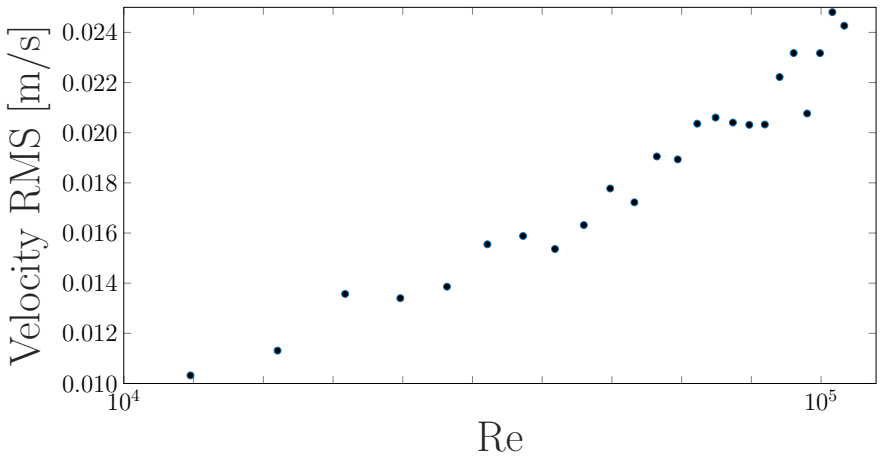

Figure 3.4. RMS values of the experimental velocity data sets taken at the end of a plate with a length and width of 14.25 cm and a thickness of 2.41 mm attached to a cylinder with a diameter of 2.85 cm and length of 14.25 cm. The flow speed is varied from 0.44 m/s to 3.8 m/s in increments of 0.15 m/s.

Dye visualization is desired to get a better understanding of how the plate is interacting with the cylinder (see Fig. 3.5). The dye is injected upstream at a flow speed of 0.1 m/s. Prior work [20, 35] has observed constructive and destructive vortex interaction modes when a plate is placed in the wake of a cylinder. However, in Fig. 3.5 the vortices look suppressed indicating that the plate is acting as a splitter plate. A splitter plate is a device used to alter the drag force of a cylinder. The splitter plate can be either attached or detached from the cylinder, and depending on the size of the plate and distance between the cylinder and the plate, the drag force is either increased or decreased [38]. In a previous study, Roshko [39] observed flow changes when splitter plates were placed behind a cylinder. He found that when the plate was attached to a cylinder and the length was five times longer than the diameter of the cylinder, vortex shedding was fully suppressed and disappeared. Given that the length of the current plate is five times the diameter of the cylinder, it is understandable the model is acting in such a way.

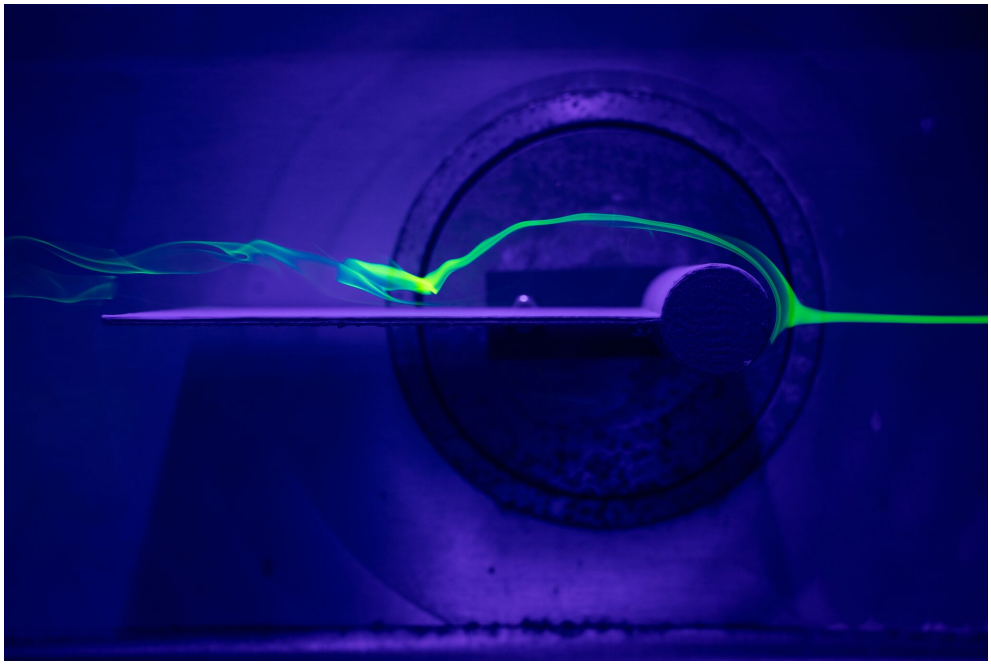

Figure 3.5. Dye visualization of a plate with a length and width of 14.25 cm and thickness of 2.41 mm attached to a cylinder with a diameter of 2.85 cm and length of 14.25 cm at a flow speed of 0.1 m/s

.

3.2.3 Drag Measurements

A force balance is used to measure the steady drag force on the plate. For this experiment, the force balance is primarily used to observe the overall drag force on the beam and relate this measurement to thrust.

3.2.3.1 Force Balance System

Strain gauges are attached to the force balance system outside of the test section of the water tunnel. When forces act on the system, a strain is created. When strain is applied to the strain gauge, it increases the resistance of the strain gauge. The change in electrical resistance is measured and converted to a force measurementt. A data acquisition program then reads the lift and drag measurements relating them to thrust. Currently, the force balance system is able to accurately measure fluid forces up to 178 N and as low as 2

N. When designing the model, the length of the cylinder was made equal to the width of the body to ensure that the resulting force was greater than the limit even at low speeds. This made the physical model more like a plate than the beams that were analyzed in the previous chapter.

3.2.3.2 Method

The bare cylinder is secured to the hydrofoil rod of the force balance system, and the flow speed is varied from 0.44 m/s to 3.8 m/s in increments of 0.15 m/s. The drag force of the cylinder, $F_{D,C}$, is measured at each flow speed. The test is then repeated to measure the drag forces for the cylinder and plate, $F_{D,CP}$. The plate's performance is then calculated in the form of the coefficient of drag, C_D, which is defined as [1]

$$C_D = \frac{F_D}{\frac{1}{2}\rho_f U^2 L_C D}, \tag{3.5}$$

where L_C is the length of the cylinder, D is the diameter.

3.2.3.3 Results

The initial assumption was that the test cylinder would show a similar a C_D trend as a smooth cylinder. However, from Fig. 3.6 this assumption did not hold true. The test cylinder did not match the trend because, through 3D printing, a surface roughness was created.

There is not a reduction in C_D when adding the plate to the cylinder, as shown in Fig. 3.7. The absence of drag reduction is in contrast to the results found in prior studies with splitter plates. Roshko [39] observed a significant reduction in the drag of a cylinder with the addition of a splitter plate. He found that when the vortex shedding disappeared, drag is reduced which did not occur in the present experiment.

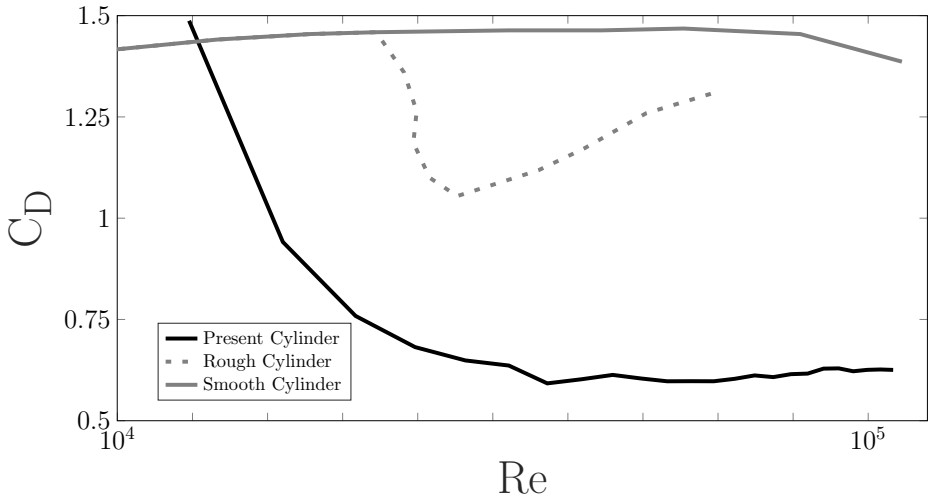

Figure 3.6. Drag coefficient values for the present cylinder compared to that of a smooth and rough cylinder from a previous study [2]. The present cylinder has a diameter of 2.85 cm and length of 14.25 cm. The drag force of the cylinder is measured over a flow speed range of 0.44 m/s to 3.8 m/s.

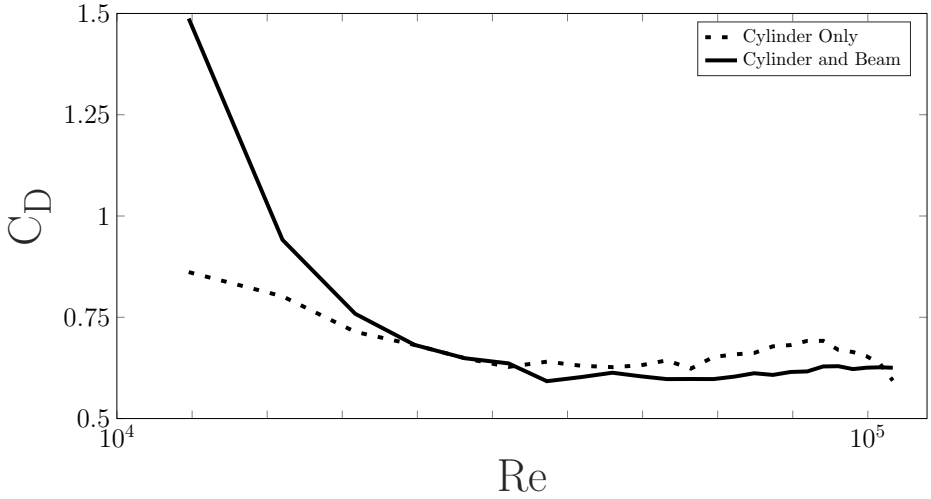

Figure 3.7. Drag coefficient values for a bare cylinder with a length of 14.25 cm and diameter of 2.85 cm and a plate with a length and width of 14.25 cm and thickness of 2.41 mm attached to a cylinder with a length of 14.25 cm and diameter of 2.85 cm over a flow speed range of 0.44 m/s to 3.8 m/s.

The results presented in Fig. 3.6 and Fig. 3.7 seem implausible. The drag force data obtained is believed to be unreliable. More testing of the force balance system is required. Future work will include comparative testing on the force balance system with a smooth cylinder. The results from these tests will then be compared to other work to get a better understanding of the force balance system.

Chapter 4

Conclusions

4.1 Summary of Main Results

This thesis explores the use of vortex energy capture as a propulsion strategy in underwater swimmers. An analytical approach is presented; a cantilever beam subject to vortex induced excitation is used to model a swimming fish in a Kármán street. The wake is represented by a moving load pattern of alternating forces. The analytical model indicates maximum thrust occurs when the length of the beam is five times the diameter of the cylinder.

A preliminary experiment was conducted to further understand the hydrodynamic relationship between a splitter plate attached to a cylinder. This configuration can be loosely compared to a fish swimming in the immediate wake of a cylinder. Through dye visualization, the splitter plate was found to suppress the vortex shedding of the cylinder. This is because the plate is five times the diameter of the cylinder. These results are in concurrence with Roshko [39]. From velocity data, the splitter plate seems to experience constant fluctuations between what Shukla et al. [37] termed mode I and mode II. Using a force balance system, drag reduction is not observed with the addition of a splitter plate. The absence of drag reduction is in contrast to prior studies which find a significant reduction in drag with the addition of a splitter plate.

4.2 Recommended Future Work

The analytical method developed in Chapter 2 studies the dynamic response of a flexible cantilevered beam subject to a periodic moving load. It is only a first step toward further understanding vortex energy capture. The next step is to extend the model to solve for thrust.

Currently, the analytical model only considers the vortices shed off of the cylinder and does not recognize the effects of the beam's vortices. However, the interaction between the two vortices contributes greatly to thrust generation [20]. Future developments to the model will include making the cylinder and beam a two-way coupled system.

Based on the results from Chapter 2, a set of experiments will be designed to physically model Fig. 2.1. As with the analytical model, the experimental approach will place a flexible beam in the wake of a Kármán street for optimal thrust generation. To produce this wake pattern, a cylinder is horizontally mounted in fluid flow. Previous work found that maximum thrust is produced with maximum response amplitude [40]. From Fig. 2.7, the model should experience maximum deflection at $\frac{L}{\Delta x} = 1$ or $\frac{D}{StL} = 1$. Assuming $St = 0.2$, the experimental model will be designed with a beam length five times the diameter of the cylinder. Because it is believed the material of the cylinder is the cause of the cylinder not showing similar behavior to that of a smooth cylinder, the cylinder will be designed with a different material, such as acrylic. Additional experiments will be performed varying the shape of the tail and the ratio of $\frac{L}{\Delta x}$.

Bibliography

[1] E. Naudascher and D. Rockwell, *Flow-Induced Vibrations: An Engineering Guide*. Dover Civil and Mechanical Engineering, Dover Publications, 2012.

[2] E. Achenbach and E. Heinecke, "On vortex shedding from smooth and rough cylinders in the range of reynolds numbers 6× 10 3 to 5× 10 6," *Journal of fluid mechanics*, vol. 109, pp. 239–251, 1981.

[3] J. C. Liao, D. N. Beal, G. V. Lauder, and M. S. Triantafyllou, "Fish exploiting vortices decrease muscle activity," *Science*, vol. 302, no. 5650, pp. 1566–1569, 2003.

[4] D. N. Beal, *Propulsion through wake synchronization using a flapping foil*. PhD thesis, Massachusetts Institute of Technology, 2003.

[5] D. Beal, F. Hover, M. Triantafyllou, J. Liao, and G. Lauder, "Passive propulsion in vortex wakes," *Journal of Fluid Mechanics*, vol. 549, pp. 385–402, 2006.

[6] K. A. Harper, M. D. Berkemeier, and S. Grace, "Modeling the dynamics of spring-driven oscillating-foil propulsion," *IEEE Journal of Oceanic Engineering*, vol. 23, no. 3, pp. 285–296, 1998.

[7] P. W. Webb *et al.*, "Hydrodynamics and energetics of fish propulsion," *Bulletin of the Fisheries Research Board of Canada*, vol. 190, pp. 1–158, 1975.

[8] I. Borazjani and F. Sotiropoulos, "On the role of form and kinematics on the hydrodynamics of self-propelled body/caudal fin swimming," *Journal of Experimental Biology*, vol. 213, no. 1, pp. 89–107, 2009.

[9] M. Saadat, F. E. Fish, A. Domel, V. Di Santo, G. Lauder, and H. Haj-Hariri, "On the rules for aquatic locomotion," *Physical Review Fluids*, vol. 2, no. 8, p. 083102, 2017.

[10] G. V. Lauder, E. J. Anderson, J. Tangorra, and P. G. Madden, "Fish biorobotics: kinematics and hydrodynamics of self-propulsion," *Journal of Experimental Biology*, vol. 210, no. 16, pp. 2767–2780, 2007.

[11] E. D. Tytell, "Median fin function in bluegill sunfish lepomis macrochirus: streamwise vortex structure during steady swimming," *Journal of Experimental Biology*, vol. 209, no. 8, pp. 1516–1534, 2006.

[12] M. Hultmark, M. Leftwich, and A. J. Smits, "Flowfield measurements in the wake of a robotic lamprey," *Experiments in Fluids*, vol. 43, no. 5, pp. 683–690, 2007.

[13] J. Yu, M. Tan, S. Wang, and E. Chen, "Development of a biomimetic robotic fish and its control algorithm," *IEEE Transactions on Systems, Man, and Cybernetics, Part B (Cybernetics)*, vol. 34, no. 4, pp. 1798–1810, 2004.

[14] B. P. Epps, P. V. Y Alvarado, K. Youcef-Toumi, and A. H. Techet, "Swimming performance of a biomimetic compliant fish-like robot," *Experiments in Fluids*, vol. 47, no. 6, p. 927, 2009.

[15] D. Barrett, M. Triantafyllou, D. Yue, M. Grosenbaugh, and M. Wolfgang, "Drag reduction in fish-like locomotion," *Journal of Fluid Mechanics*, vol. 392, pp. 183–212, 1999.

[16] J. Gray, "Studies in animal locomotion: I. the movement of fish with special reference to the eel," *Journal of experimental biology*, vol. 10, no. 1, pp. 88–104, 1933.

[17] U. Müller, B. Van Den Heuvel, E. Stamhuis, and J. Videler, "Fish foot prints: morphology and energetics of the wake behind a continuously swimming mullet (chelon labrosus risso)," *Journal of Experimental Biology*, vol. 200, no. 22, pp. 2893–2906, 1997.

[18] J. C. Liao, "A review of fish swimming mechanics and behaviour in altered flows," *Philosophical Transactions of the Royal Society B: Biological Sciences*, vol. 362, no. 1487, pp. 1973–1993, 2007.

[19] K. D. Fausch, "Profitable stream positions for salmonids: relating specific growth rate to net energy gain," *Canadian Journal of Zoology*, vol. 62, no. 3, pp. 441–451, 1984.

[20] R. Gopalkrishnan, M. Triantafyllou, G. Triantafyllou, and D. Barrett, "Active vorticity control in a shear flow using a flapping foil," *Journal of Fluid Mechanics*, vol. 274, pp. 1–21, 1994.

[21] G. V. Lauder, J. Lim, R. Shelton, C. Witt, E. Anderson, and J. L. Tangorra, "Robotic models for studying undulatory locomotion in fishes," *Marine Technology Society Journal*, vol. 45, no. 4, pp. 41–55, 2011.

[22] G. V. Lauder, B. Flammang, and S. Alben, "Passive robotic models of propulsion by the bodies and caudal fins of fish," *Integrative and Comparative Biology*, vol. 52, no. 5, pp. 576–587, 2012.

[23] M. Triantafyllou, G. Triantafyllou, and R. Gopalkrishnan, "Wake mechanics for thrust generation in oscillating foils," *Physics of Fluids A: Fluid Dynamics*, vol. 3, no. 12, pp. 2835–2837, 1991.

[24] G. S. Triantafyllou, M. Triantafyllou, and M. Grosenbaugh, "Optimal thrust development in oscillating foils with application to fish propulsion," *Journal of Fluids and Structures*, vol. 7, no. 2, pp. 205–224, 1993.

[25] S. Law, T. H. Chan, and Q. Zeng, "Moving force identification: a time domain method," *Journal of Sound and Vibration*, vol. 201, no. 1, pp. 1–22, 1997.

[26] S. Law, T. H. Chan, and Q. Zeng, "Moving force identification—a frequency and time domains analysis," *Journal of Dynamic Systems, Measurement, and Control*, vol. 121, no. 3, pp. 394–401, 1999.

[27] M. Olsson, "Finite element, modal co-ordinate analysis of structures subjected to moving loads," *Journal of Sound and Vibration*, vol. 99, no. 1, pp. 1–12, 1985.

[28] E. Esmailzadeh and M. Ghoreyshi, "Vibration analysis of a timoshenko beam subjected to a travelling mass," *Journal of Sound and Vibration*, vol. 199, no. 4, pp. 615–628, 1997.

[29] P. Lou, G. Dai, and Q. Zeng, "Finite-element analysis for a timoshenko beam subjected to a moving mass," *Proceedings of the Institution of Mechanical Engineers, Part C: Journal of Mechanical Engineering Science*, vol. 220, no. 5, pp. 669–678, 2006.

[30] C. Bilello, L. A. Bergman, and D. Kuchma, "Experimental investigation of a small-scale bridge model under a moving mass," *Journal of Structural Engineering*, vol. 130, no. 5, pp. 799–804, 2004.

[31] U. Lee, "Revisiting the moving mass problem: onset of separation between the mass and beam," *Journal of Vibration and Acoustics*, vol. 118, no. 3, pp. 516–521, 1996.

[32] D. L. Logan, *A first course in the finite element method*. Cengage Learning, 2011.

[33] P. Kundu, I. Cohen, and D. Dowling, *Fluid Mechanics*. Elsevier Inc., 2016.

[34] M. Oyeyemi, *The design and qualification of the UGA water tunnel*. PhD thesis, The University of Georgia, 2018.

[35] J. Wu and C. Shu, "Numerical study of flow characteristics behind a stationary circular cylinder with a flapping plate," *Physics of Fluids*, vol. 23, no. 7, p. 073601, 2011.

[36] R. D. Blevins, *Formulas for dynamics, acoustics and vibration*. John Wiley & Sons, 2016.

[37] S. Shukla, R. Govardhan, and J. Arakeri, "Dynamics of a flexible splitter plate in the wake of a circular cylinder," *Journal of Fluids and Structures*, vol. 41, pp. 127–134, 2013.

[38] Q. Xiao, K. Sun, H. Liu, and J. Hu, "Computational study on near wake interaction between undulation body and a d-section cylinder," *Ocean Engineering*, vol. 38, no. 4, pp. 673–683, 2011.

[39] A. Roshko, "On the wake and drag of bluff bodies," *Journal of the Aeronautical Sciences*, vol. 22, no. 2, pp. 124–132, 1955.

[40] F. Paraz, L. Schouveiler, and C. Eloy, "Thrust generation by a heaving flexible foil: Resonance, nonlinearities, and optimality," *Physics of Fluids*, vol. 28, no. 1, p. 011903, 2016.